Dipolar ordering and glassy freezing in methanol-β-hydroquinone-clathrate

H. Woll,[1] M. C. Rheinstädter,[1] F. Kruchten,[1] K. Kiefer,[1] M. Enderle,[1,2] A. Klöpperpieper,[1] J. Albers,[1] and K. Knorr[1]
[1]*Technische Physik, Universität des Saarlandes, 66041 Saarbrücken, Germany*
[2]*Institut Max von Laue–Paul Langevin (ILL), Boîte Postale 156, F33042 Grenoble Cedex 9, France*
(Received 5 September 2000; published 14 May 2001)

The dielectric, structural, and thermodynamic properties of single crystals of methanol-β-hydroquinone-clathrates have been studied as function of temperature and of the concentration x of the polar guest molecules. At higher temperatures the dielectric response along the threefold crystal axis is of the quasi-one-dimensional Ising type. At lower temperatures the higher concentrated samples order antiferroelectrically whereas the lower concentrated ones freeze into dipole glasses. The behavior is interpreted in terms of the methanol dipole moments coupled by the electric dipole-dipole interaction which is highly frustrated because of the rhombohedral symmetry of the lattice. The dielectric relaxations have been analyzed.

DOI: 10.1103/PhysRevB.63.224202 PACS number(s): 76.30.Kg, 64.60.Cn, 64.70.Pf, 77.22.Ch

INTRODUCTION

Our understanding of collective ordering transitions in crystals mainly stems from magnetic systems. In favorable cases the full magnetic structure and dynamics can be deduced from relatively little information: the magnitude of the elementary magnetic dipole moment (the ''spin'') of the individual d or f ion and the exchange interaction as specified by the coupling parameters to some few neighbor spins. Even the spin glass state of dilute magnetic systems has been successfully simulated on this basis, $Eu_xSr_{1-x}S$ being a prominent example.[1] The understanding of electric dipolar, e.g., ferroelectric ordering let alone the freezing into the dipolar glass state[2] is much more rudimentary. Usually neither the elementary dipole moments nor the interactions between them are known. This is obvious for crystal in which the electric polarization results from displacements of one sublattice with respect to the other. Here the knowledge of the full lattice dynamics including anharmonicities is required. Orientational order-disorder transition appear to be somewhat simpler and closer to magnetic systems. But even here the dipole moment of the active molecular unit is usually dressed by a polarization and strain cloud of the lattice, thus making a distinction between the direct interactions between individual dipole moments and lattice mediated interactions difficult.

This article deals with a cage compound, namely methanol-β hydroquinone,[3] in which—as we will show—well defined electric dipole moments, namely those of the methanol guest molecules, are well decoupled from the host lattice and interact via a well defined interaction, namely the electric dipole-dipole (EDD) interaction. In this sense these clathrates are conceptually very close to magnetic systems.

In the β-modification the H-bonded lattice of the quinol HO-C_6H_4-OH molecules leaves space for and is stabilized by neutral guest molecules of appropriate size. The lattice is rhombohedral with three hydroquinone molecules and one cage filled by one guest molecule in the unit cell. The sidewalls of the cage are formed by the aromatic rings of six quinol molecules, top and bottom of the cage by regular hexagons of oxygen atoms with a proton on each O-O bond (Fig. 1). Possible guests range from molecules as small as Ar to molecules as large as CH_3CN. For the smaller guest molecules including CH_3OH the hexagonal lattice parameters are about $a=16.6$ Å, $c=5.5$ Å and are almost independent of the size and shape of the guest molecule, suggesting that these molecules can move relatively freely in the cages. In the decades after the pioneering work of Palin and Powell[4] in the 1940s, most pertinent work was concerned with the dynamics of the individual guest molecule in the crystal field of the cavity, e.g., by optical spectroscopy. New interest in the quinol clathrates arose when Matsuo *et al.*[5,6] showed by permittivity and heat capacity experiments that the dipolar guest molecules order collectively at lower temperatures. The ordering temperatures T_s range from about 180 K for HCN to 65K for CH_3OH and 8K for H_2S. T_s was shown to scale with the square of dipole moment μ of the free molecule,[7] an observation which suggests that the ordering is due to the EDD interaction.

For the present study we have chosen the methanol clathrate. The methanol guest molecule has a reasonably large dipole moment of 1.69D. Large single crystals can be grown with a controlled fractional occupancy x of the cavities. In fact the host lattice tolerates fractional occupations x down to 0.34 before collapsing. T_s decreases with decreasing x and eventually below a critical concentration x_c of about 0.75 the transition no longer occurs.[6,8] Of direct relevance for our

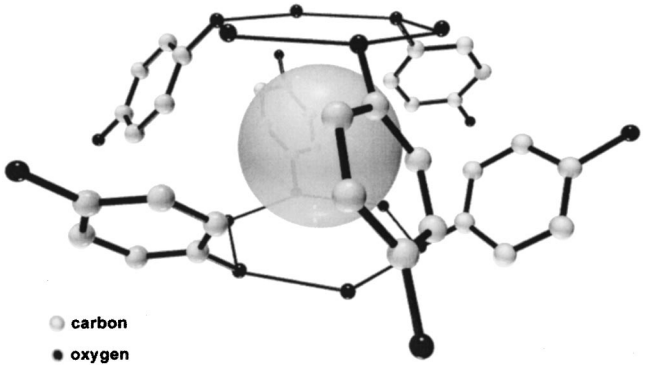

FIG. 1. Schematic view of a cage in the β-quinol structure. O atoms are shown black, C atoms white, and the H atoms of the hydroxyl groups reside on the bonds between O atoms.

study are previous heat capacity measurements[6] for a series of samples with different x and NMR studies on the fully concentrated methanol clathrate[9,10] which give insight into the orientation and the reorientational dynamics of the guest molecule. There are also some reports on the permittivity,[6,11] but the information on the dielectric response has been by no means complete. The articles of Dansas and Sixou[12] review the state of the field in 1976 and give a valuable insight into some aspects of the hydrochinon clathrates.

We have shown recently[8] that clathrates with lower methanol concentrations freeze into the dipole glass state. This state is usually considered analogous to the spin glass state of dilute magnetic systems. Both types of glassy states are thought to result from the random occupation of lattice sites by (electric or magnetic) dipole moments in combination with the frustrated nature of the interaction.[1,2]

In this article we will give a full report on our permittivity results, including an analysis of the dielectric relaxations, as well as complementary sample characterization by x-ray diffraction, heat capacity and birefringence measurements.

EXPERIMENT

We have grown single crystals with $x=0.97$, 0.84, 0.79, 0.73, 0.50, 0.40 from a saturated solution of quinol, methanol and *n*-propanol at 313 K. The propanol molecule is too big in order to be incorporated in the cavities, but the propanol concentration controls the methanol content x of the crystals. We have checked x by density measurements, the x values quoted are accurate within 0.02 at higher x and 0.04 at lower x. For the permittivity and the optical measurements thin plates have been cut and polished subsequently on cloth soaked with methanol. Two cuts have been used, with the plate normal along (ab plates) and perpendicular to the c axis (ac plates). (If not stated otherwise, we use the hexagonal notation.) The cuts are accurate to $\pm 2°$. When kept in air, the surfaces of the samples deteriorate within hours because of the evaporation of methanol (what one can smell) which presumably leads to a transformation of the surface layers into the α modification. For the permittivity and birefringence measurements which rely on intact surfaces we have therefore protected the surface by evaporating gold layers. For the permittivity measurements these Au layers also serve as electrodes. The sample thickness is typically 0.5 mm for measurements of ε_c with the electric field along c and 0.3 mm for ε_a with the field perpendicular to c. The top and bottom electrode are parallel to within 0.01 mm. The geometrical capacities as calculated from the thickness and the electrode area range from 0.4 to 1 pF. The complex dielectric constant has been measured with the impedance analyzers HP4274A and 4275A covering a frequency f band from 100 Hz to 1 MHz in a He-flow cryostat from room temperature down to 4 K. The three samples with lower concentrations have been investigated additionally in the group of A. Loidl at the university of Augsburg down to frequencies of 10 mHz with the frequency analyzer FRA 1260 in combination with a Chelsea interface. In birefringence measurements the polarization state of the transmitted light beam has been analyzed with a Sénarmont setup. For ab plates the light beam (of a He-Ne laser) travels along c and the polarization vector lies in the basal plane whereas for ac plates the beam is perpendicular to c and the polarization is chosen at 45° with respect to c. For ab plates also pictures of the multidomain state of the higher concentrated samples at low T have been taken with the sample between crossed polarizers. For the heat capacity studies we used a setup in which the sample (about 40 mg) is placed on a sapphire plate which is equipped with a thermometer and an evaporated metal film for resistance heating. Heat capacity data are obtained point by point with the quasiadiabatic heat pulse technique. For the determination of the entropy of transformation at T_s we used a scanning technique. Here a metal wire served as thermal link between the sapphire plate and the thermal shield. Our x-ray diffraction studies concentrated on the almost fully concentrated sample, $x=0.97$. We used monochromatized Cu K_α radiation and a two-circle diffractometer which is equipped with a closed cycle refrigerator. The single crystalline samples have been usually oriented with c perpendicular to the scattering plane. This allows scans within the $(hk0)$ plane. Scans within plane (hkl), l constant, $l \leqslant 1$ are possible by moving the detector out of the diffractometer plane . Occasionally the samples have been adjusted with c in the dif-

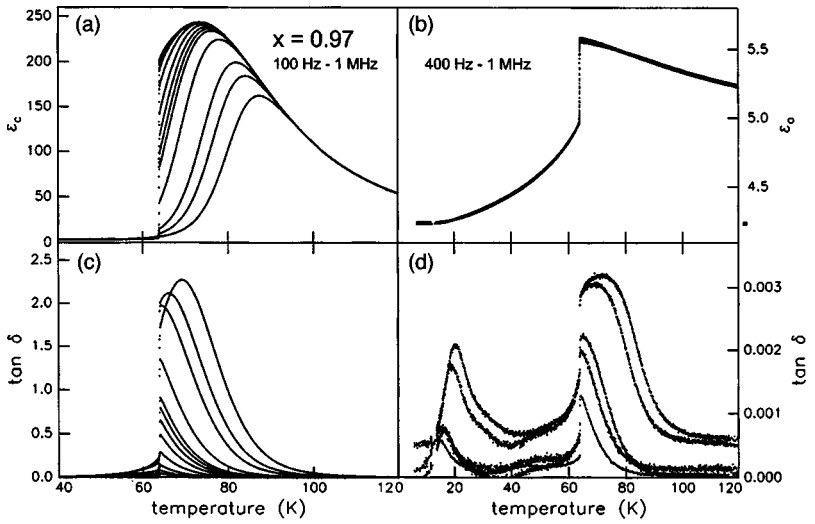

FIG. 2. The permittivity along c and a and the corresponding loss tangents as function of temperature for $x=0.97$ and a series of measuring frequencies.

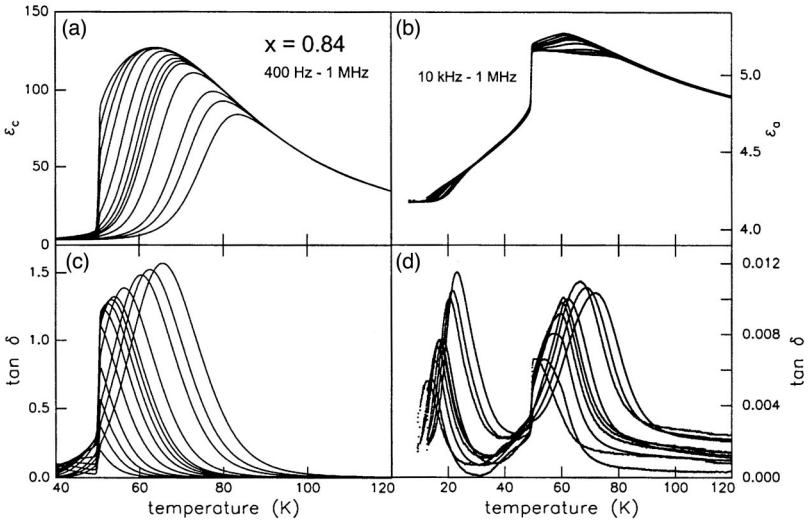

FIG. 3. Same as Fig. 2 but for $x=0.84$.

fractometer plane. Rotating crystal exposures have also been taken. Here the crystal was rotated about c and the incoming beam being perpendicular to c.

RESULTS

Figures 2–5 show the T dependence of ε_c, ε_a and the corresponding loss tangent for some measuring frequencies f of four of the six samples investigated. There are two temperature regimes of dispersion and loss, the primary one at temperatures around 60 K and the secondary one which is visible in ε_a, only, at about 20 K. For the higher concentrated samples there is an almost vertical drop, both in ε_c and ε_a, at the transition temperature T_s. For $x=0.97$ several plates have been cut from different parts of a large single crystal. The T_s values are identical within 0.1 K, suggesting that there are no major gradients of the methanol concentration in the crystal. This is also supported by the rather sharp, almost vertical drop of ε_c and ε_a at T_s, not only for $x=0.97$, but also for $x=0.84$ and 0.79. On the other hand, the ε_a measurements on different plates differ somewhat with respect to the value of the loss in the temperature range of the primary relaxations. We relate these effects to an imperfect cutting of the plates and show in Fig. 2 the results on the plate for which the loss is smallest. The transition temperatures of Table I are from dielectric measurements as obtained on cooling. T_s values from the other types of experiment agree within 1 K. Measurements of the electric polarization P as function of the electric field E along c on $x=0.97$ show linear behavior up to the maximum field of 40 kV/cm. The samples are of excellent optical quality with no apparent sign of stress birefringence. Figure 6 shows a picture of an ab plate in the low-T multidomain state ($T=63$ K, $x=0.97$) which develops below T_s. Obviously the domain walls meet at angles of 60° within the basal plane. There is a well defined azimuthal setting of the crossed polarizers for which the light passing along c through a given domain is extinguished. The azimuth angles of the three domains differ by 60°. This means that the one of the principal axes of the optical tensor lies in the former basal plane or is at least close to it, and that this tensor is rotated by 60° from one domain to the other. Thus the threefold symmetry of high-T phase is broken. The T dependence of the linear birefringence Δn is shown in Fig. 7 for both types of plates. At the phase transitions of the higher concentrated ''ordering'' samples, rep-

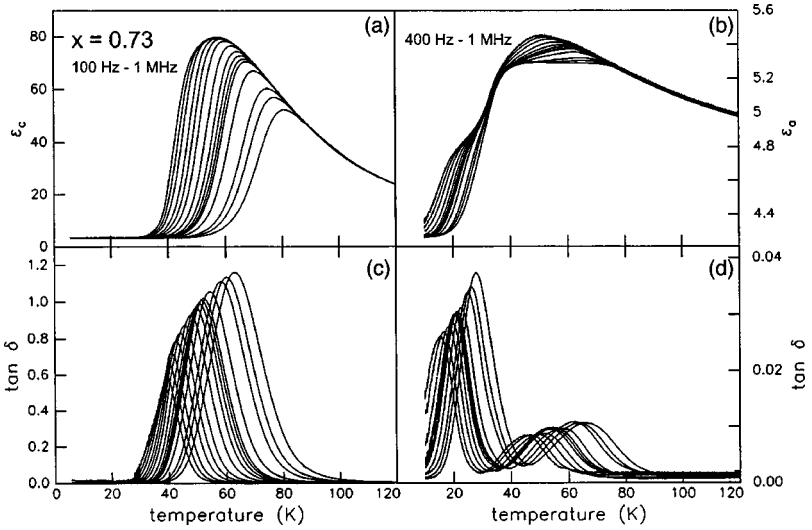

FIG. 4. Same as Fig. 2 but for $x=0.73$.

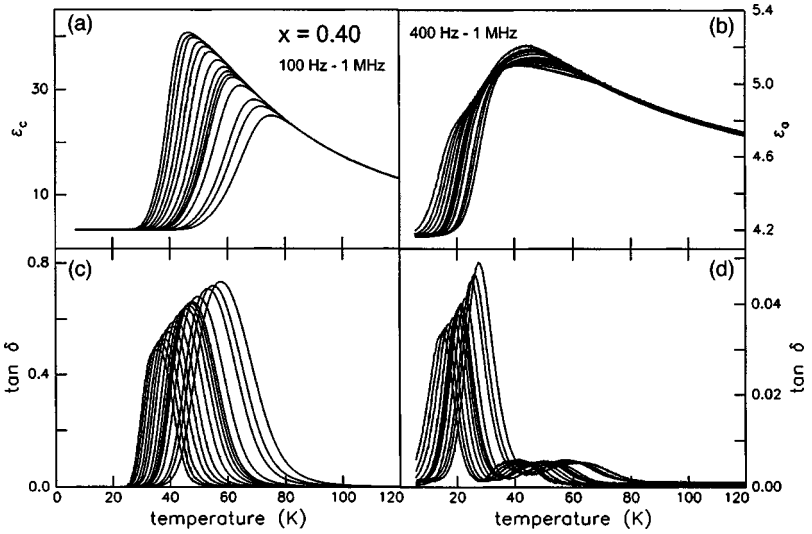

FIG. 5. Same as Fig. 2 but for $x=0.40$.

resented in Fig. 7 by $x=0.97$, both Δn_{ab} and Δn_{ac} show a jump at T_s. For $T<T_s$ spots have been selected where one could be reasonably sure that the light beam on its way through the sample stays within one domain. In the rhombohedral phase Δn_{ab} vanishes as required by the threefold symmetry axis. The finite value of Δn_{ab} below T_s is due to the loss of this symmetry element in the low temperature phase. In the ''non-ordering'' samples (represented in Fig. 7 by $x=0.40$) there is no birefringence within the basal plane down to lowest temperatures and in fact the nulling of the light intensity for crossed polarizers does not deteriorate towards low *T*. The overall variation of Δn_{ac} between high and low temperatures roughly scales with the methanol content.

The heat capacity of three samples as obtained with the quasiadiabatic technique is presented in Fig. 8. The phase transitions for $x=0.97$ and 0.79 show up as sharp almost δ-like anomalies. Figure 9 shows data on the evolution of the entropy *S* across the phase transition for $x=0.97$ as obtained with the scanning technique, both for cooling and heating. The altogether steplike *T* dependence and the slight thermal hysteresis, $\Delta T=0.2$ K, suggests that the transition is of first order. The small wiggles which can be seen in the trace of the left panel of Fig. 9 are presumably due to a coexistence of the high-*T* and the low-*T* phase in which the two coexisting phases adjust to the changing temperature by discrete jumps of the phase boundaries and the domain walls. (Coexisting phases and instantaneous adjustments of boundaries have been also observed with the optical setup.) Figure 9 shows the anomalous part of S(T), i.e., the entropy of transformation which is obtained by subtracting a suitable smooth background. As can be seen, the anomalous part extends to temperatures some degrees below T_s.

TABLE I. The phase transition temperature T_s, the intrachain J_c and the interchain $J_\perp$ coupling parameter, and the Arrhenius barrier E_B (all in units of K) as functions of the methanol occupancy *x*.

x	0.97 ($\pm$0.02)	0.84	0.79	0.73	0.50	0.40
T_s	63.9 ($\pm$0.1)	50.3	45.2			
J_c	195 ($\pm$5)	175	176	155	121	111
$J_\perp$	-0.3 ($\pm$0.2)	-1.6	-2.2	-3.2	-6.1	-7.5
E_B	848 ($\pm$15)	833	830	831	820	815

Our x-ray diffraction study on the sample with $x=0.97$ concentrates on the changes of the lattice parameters induced by the phase transition and the search for the superlattice reflections in the low *T* phase. Our equipment does not allow the sampling of a sufficient number of Bragg intensities for a rigorous determination of the crystal structure. Rotating crystal exposures on the rhombohedral phase show layers of reflections (hkl), $l=$const and integer. In the low-*T* phase there are additional reflections in layers with integer and half-integer values of *l*. The superlattice points are linear combinations of two zone boundary wave vectors, belonging to different stars of equivalent vectors, namely $\mathbf{q}_1=(\frac{1}{2}\frac{1}{2}\frac{1}{2})_{rh}$ and $\mathbf{q}_2=(\frac{1}{2}\frac{1}{2}0)_{rh}$, in rhombohedral notation. A number of such superlattice reflections have been scanned on the diffractometer. The *T* dependence of the intensity of two such reflections is shown in Fig. 10. The square root of these intensities are measures of the primary order parameter of the phase transition. From these results the phase transition

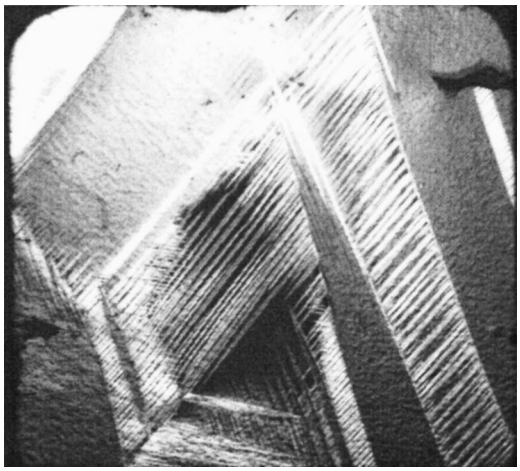

FIG. 6. Photograph of the multidomain state of the low-*T* phase, seen along *c* through crossed polarizers.

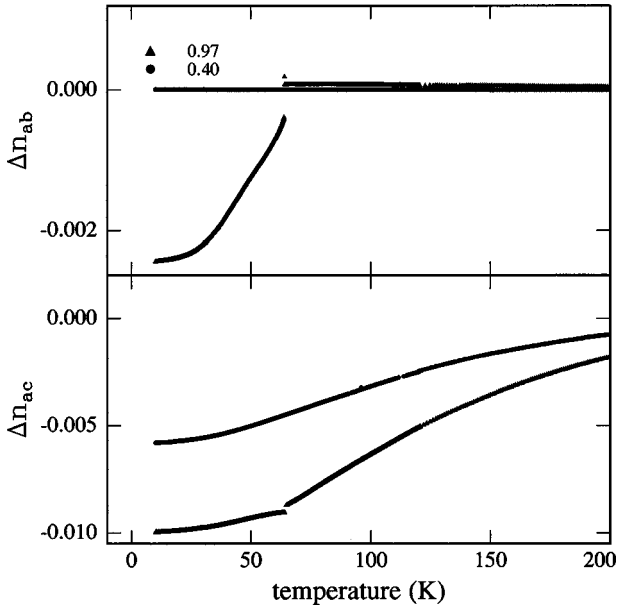

FIG. 7. The linear birefringence, Δn_{ac} and Δn_{ab}, as function of temperature for $x=0.97$ and 0.40.

has to be classified as being of weakly first order. The second point of interest is the spontaneous strain of the lattice in the low-T phase. The principal reflections split into three product reflections, the positions of which are at the corners of small triangles in reciprocal space centered at the parent reflection. Each product reflection represents one of the three domains of the low-T state. Because of the finite resolution of the diffractometer, scans through the original reciprocal lattice points of the high-T phase along suitable directions collect most of the intensity of the product reflections. Figure 11 shows pertinent results. Here the (600) and the (003) reflection are probed by a rocking scan within the ($hk0$) and the ($h0l$) zone, respectively. The figure also illustrates one peculiarity of the transition. The statistical weights of the three domains, as represented by the intensities of the product peaks, vary from one cooling-heating cycle to the next and

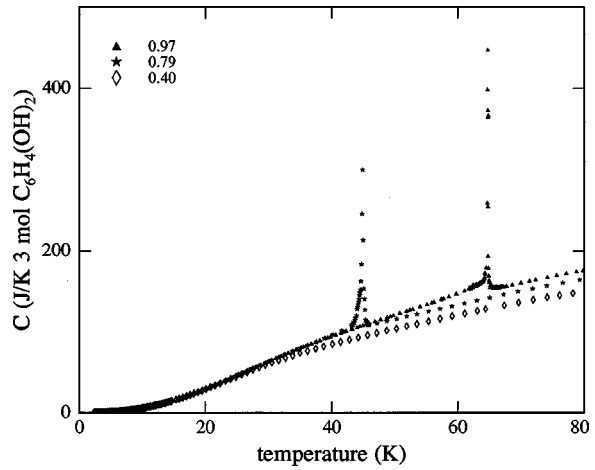

FIG. 8. The heat capacity per cage, which is formed by three quinol molecules, as function of temperature for $x=0.97$, 0.79, and 0.40.

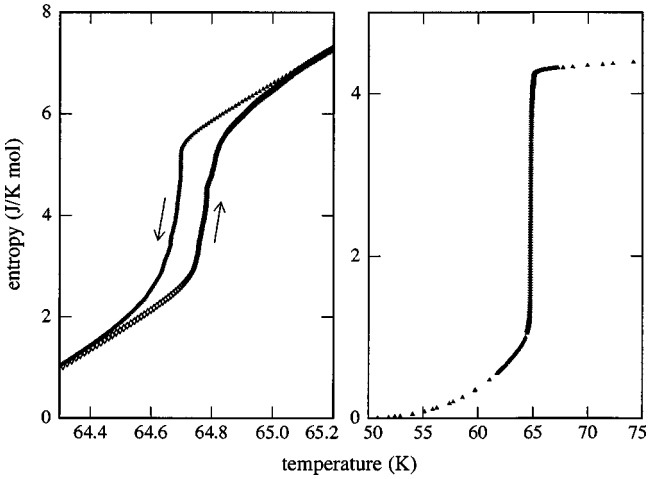

FIG. 9. Entropy as function of temperature for $x=0.97$. The left panel shows data as derived directly from scanning calorimetry on cooling and heating; in the right panel a suitable chosen linear background has been subtracted. Note the different temperature scales of the panels.

also change within a cycle. Usually only two and occasionally just one of the three domains carries significant weight. For this reason the results of two cycles on the (600) reflection are superimposed in the figure. It thus appears that a favorable matching of the domains is difficult. The peak positions as deduced from Fig. 11 are shown in Fig. 12. For a more accurate determination of the peak positions we carried out grid scans within the chosen scattering plane. Possible minor excursion of the peaks out of the plane remain undetermined. The major elements of the spontaneous deformation of the lattice below T_s are a tilt $\Delta\beta^*$ of c^* axis towards a^*, a change $\Delta\gamma^*$ of the angle between a^* and b^* to a

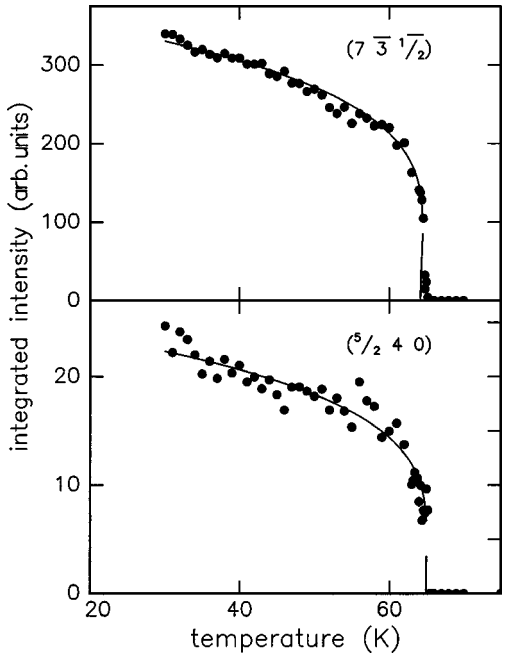

FIG. 10. The temperature dependence of the intensities of two superlattice reflections of the low-temperature phase, $x=0.97$.

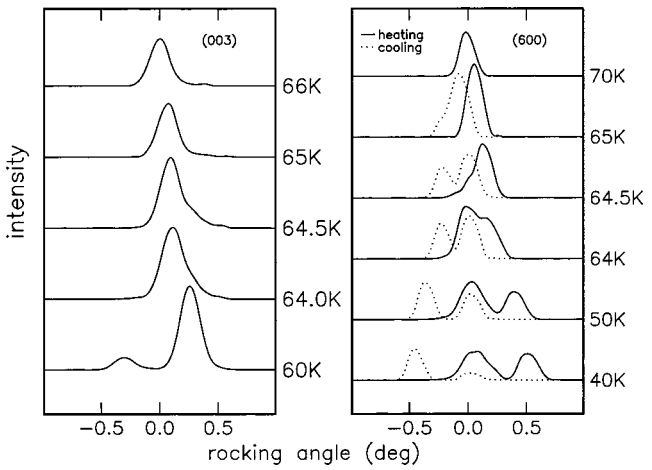

FIG. 11. Rocking scans of two Bragg reflections for several temperatures, $x=0.97$.

value lower than 60° and a lengthening of a^*, $\epsilon=(a-a')/a$. The shear angles are found to be $\Delta\beta^*=0.63°$, $\Delta\gamma^*=0.46°$, $\epsilon=0.010$ ($T=30$ K). The resulting tensor of the symmetry breaking part of the spontaneous deformation (Aizu tensor[13]) is

$$\begin{pmatrix} -\frac{1}{2}\left(\epsilon+\frac{\Delta\gamma^*}{\sqrt{3}}\right) & \frac{1}{2}\left(\frac{\epsilon}{\sqrt{3}}-\frac{4}{3}\Delta\gamma^*\right) & -\frac{1}{2}\Delta\beta^* \\ & \frac{1}{2}\left(\epsilon+\frac{\Delta\gamma^*}{\sqrt{3}}\right) & 0 \\ & & 0 \end{pmatrix}. \tag{1}$$

The volume contracts by 0.1% across T_s.

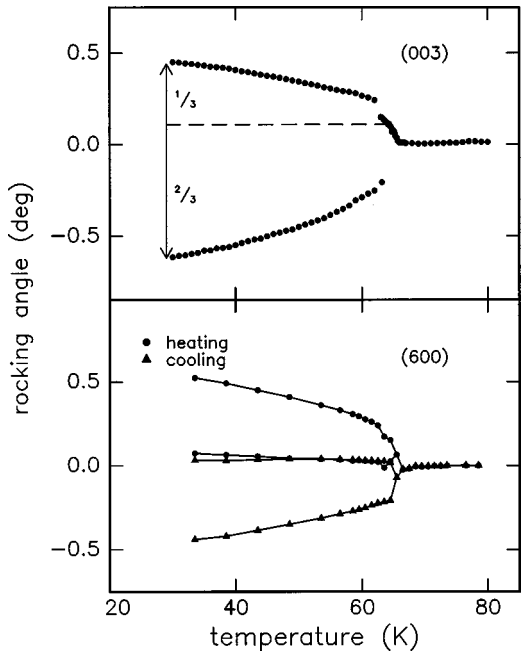

FIG. 12. The splitting of two Bragg reflections as function of temperature, as derived from the scans of Fig. 11.

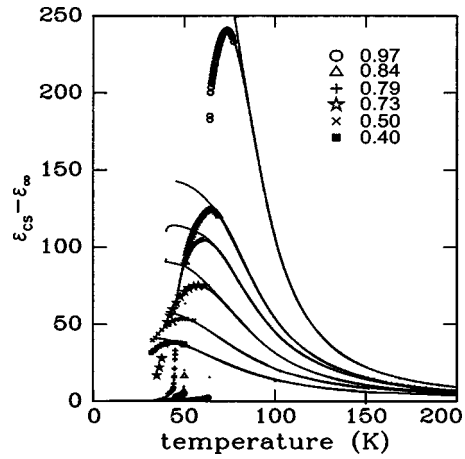

FIG. 13. The static permittivity along c as function of temperature of all samples investigated. The solid lines are fits of the quasi-one-dimensional Ising model. The data points at higher temperatures, which coincide practically perfectly with the fits, have been measured directly; those at lower temperatures, which are shown by symbols, are from the HN analysis of the dispersive regime. From Woll *et al.* (Ref. 8).

ANALYSIS OF THE PERMITTIVITY DATA

At higher T the permittivity is independent of the measuring frequency and thus represents the static permittivity. At lower T, static values ε_{cs} of the permittivity ε_c have been obtained from the analysis of the relaxational behavior (see below). For all samples the high temperature data on ε_{cs} deviate significantly from a Curie-Weiss law, as has been already noted previously by Murakami *et al.*[11] for a sample which was considered fully concentrated, even though T_s and the maximum value of ε_c was slightly lower than for the present $x=0.97$ sample. The T dependence of ε_{cs} of all samples can be almost perfectly fitted by $(\varepsilon_{cs}-\varepsilon_\infty)^{-1}=T[\exp(-2J_c/T)-J_\perp/T]/M_c$ from room temperature down to about 75 K for $x=0.97$ and 50 K for $x=0.40$, for example. See Fig. 13. This expression is based on the exact treatment of an Ising chain with next-neighbor coupling J_c and the mean field treatment of the coupling $J_\perp$ between the chains.[14] $M_c=n\mu_c^2/\varepsilon_0$ where n is the density of the dipoles and μ_c the component of the dipole moment along the chain. The parameters of the best fit are given in Table I. The values obtained for ε_∞ range from 3.7 to 4.1 which agrees well with the low-T limit of the experimental data. ε_a is significantly smaller and changes little with T. Moreover contaminations by ε_c due to imperfect cutting cannot be excluded. For $x=0.97$, we have prepared several samples and for the one shown in Fig. 2 we obviously arrived at a perfect orientation, since there is hardly any frequency dependence in the T range where ε_c shows strong dispersion. This data can be fitted by a Curie-Weiss law $\varepsilon_{as}-\varepsilon_\infty=M_\perp/(T+\theta)$ with $\theta=71$ K and $M_\perp=n\mu_\perp^2/2\varepsilon_0=170$ K. $\mu_\perp$ is the component of the dipole moment perpendicular to c. The equation for $M_\perp$ applies to a moment which can reorient by jumps between three or more equally spaced azimuthal states within a plane, the electric field lying in the plane.

The frequency dependence of the permittivity along c, $\varepsilon_c=\varepsilon'+\imath\varepsilon''$, has been analyzed on the basis of the empirical

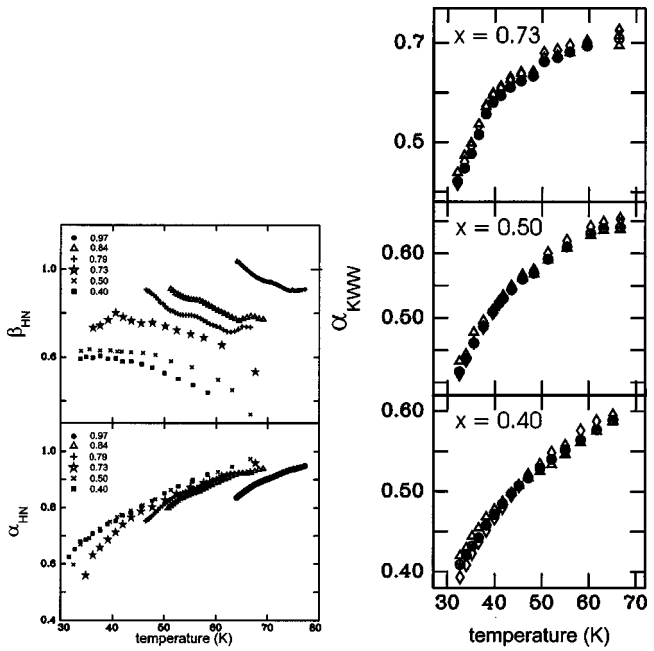

FIG. 14. The temperature dependence of the exponents of the HN and the KWW ansatz for the relaxations of ε_c.

relations of Havriliak-Negami (HN) and Kohlrausch, Williams, and Watt (KWW) and of the semiempirical model of Chamberlin.[15] The analysis with the HN-relation $\varepsilon(f)=\varepsilon_\infty+(\varepsilon_s-\varepsilon_\infty)/[1+(\imath 2\pi f\tau)^\alpha]^\beta$ is straightforward and supplies the static permittivity ε_s, or alternatively the dispersion step $\Delta\varepsilon=\varepsilon_s-\varepsilon_\infty$, an average relaxation time τ and the exponents α and β which characterize the width and asymmetry of the distribution of relaxation times $g(\tau)$. For the ordering samples the data analysis has been restricted to the paraelectric phase. The variation of α and β with T is shown in Fig. 14 for several samples. The values of the static permittivity resulting from the fits are included in Fig. 13. The relaxation time τ is found to follow an Arrhenius law $\tau=f_A^{-1}\exp(E_B/kT)$, the energy barriers E_B are given in Table I, the attempt frequencies f_A of the samples are all between 19 and 22 GHz.

The KWW ansatz refers to the time evolution of the relaxation function according to $\Phi\propto\exp(-(t/\tau)^\alpha)$, τ is again a characteristic average relaxation time and α the stretching exponent which describes decays slower than exponential. Small values of α stand for broad distributions $g(\tau)$. For the transformation of the KWW model into the frequency domain we followed the approximative treatment of Dishon *et al.*[16] This approximation limits the evaluation to frequencies above a certain lower boundary which shifts upwards the narrower $g(\tau)$. This makes fits of this model to the narrow distributions of the higher concentrated samples problematic. A KWW fit for $x=0.40$ has been shown previously.[8] Fits of the KWW model are of similar quality, for $x=0.40$ and $x=0.50$ even of slightly better quality than those based on the HN expression, even though the latter model contains one parameter more. The HN and KWW values of $\Delta\varepsilon$ and τ are practically identical. The T variation of α_{KWW} for $x=0.73,0.50,0.40$ is included in Fig. 14.

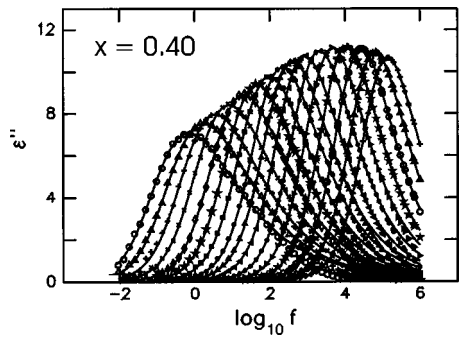

FIG. 15. The imaginary part of ε_c at several selected temperatures as function of the measuring frequency for $x=0.40$. The temperature range from 31.678 K (left) to 58.371 K (right) in steps which are equidistant on a $1/T$ scale. The solid lines are fits of Chamberlin's relaxation model to the data. See Ref. 8 for a fit of the KWW model to the same set of data.

The semiempirical model of Chamberlin[15] is based on the idea of dynamically correlated domains of size X, regions which collectively relax with a unique τ. τ depends on the size of the domain. The parameters of the model are the relaxation amplitude Φ_0, the average domain size $\langle X\rangle$ and the coefficient c which in combination with the frequency f_∞ determines the X dependence of the relaxation rate $f(X)=f_\infty\exp(-c/X)$. $c=0$ refers to the Debye case, large $c\neq 0$ means polydispersity, for $c<0$ large domains decay slower than small ones. We used the size distributions suggested by Chamberlin and obtained acceptable fits with a Gaussian distribution, whereas those based on Poisson type distributions of percolation theories turned out to be less satisfactory than HN or KWW fits. See Fig. 15 for fits to curves of ε'' vs $\log(f)$ for $x=0.40$. The T dependence of the fit parameters for $x=0.40$ is shown in Fig. 16. $\langle X\rangle/c$ changes from -0.2 to -0.1 between 60 K and 30 K. Similar values have been observed for the glassy freezing of molecular liquids such as salol, on the other hand a Gaussian distribution is—according to Chamberlin—an indication for ergodic behavior.

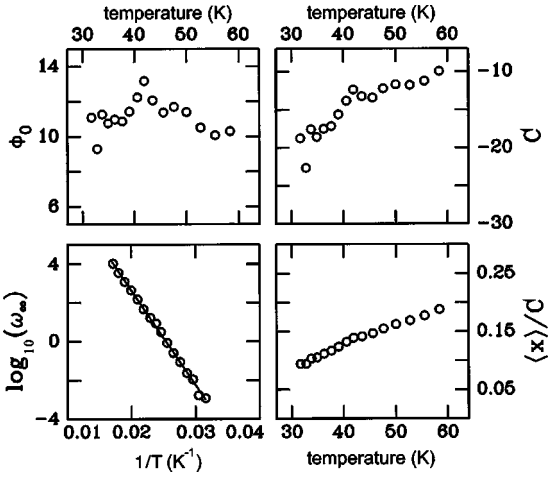

FIG. 16. The temperature dependence of the parameters of Chamberlin's relaxation model for $x=0.40$.

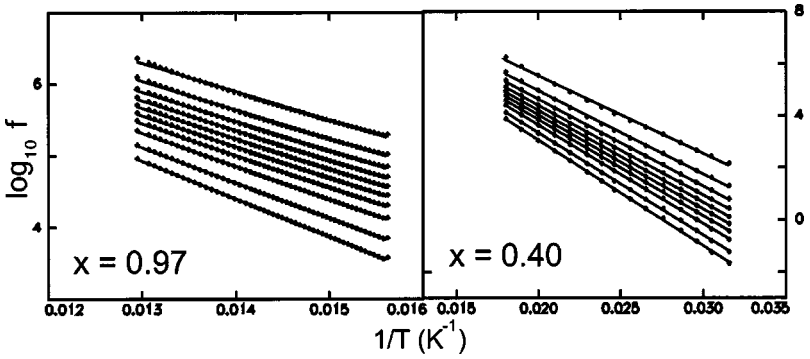

FIG. 17. The frequency vs $1/T$ relation taken at different relative heights δ of the dispersion step of ε_c for $x=0.97$ and 0.40. The δ values range from 0.1 at the top in steps of 0.1 to 0.90 to the bottom. The lowest value is $\delta=0.95$.

Several glass formers show a high-frequency tail of the permittivity where $\varepsilon''(\omega)$ varies as a power law. It has been argued that this behavior could be related to the glass transition being a phase transition in the thermodynamic sense.[17] Unfortunately our results on the high-frequency limit are not accurate enough for a meaningful analysis in terms of power laws. We can only point out that none of the models cited above supplies an acceptable fit of the high-frequency wing of $\varepsilon''(\omega)$; see Fig. 15 for the Chamberlin fit and Fig. 2 of Ref. 8 for the KWW fit.

Finally we analyzed the f,T relation at different relative heights δ of the dispersion step. For all samples, δ-values and temperatures Arrhenius laws have been obtained. The results on $x=0.97$ and 0.40 are shown in Fig. 17. This method probes a weighted $g(\tau)$ with weights of the slow relaxations increasing with δ.[18] Hence the results suggest that all relaxations occuring in the system are thermally activated.

We have also analyzed the residual relaxation of ε_c of the ordering samples just below $T_s(x)$ and the primary and secondary relaxations of ε_a. For all these cases the permittivity is only slightly larger than ε_∞ (see Figs. 2–5). Therefore the fit parameters are by far less reliable than those reported above on the primary relaxations showing up in ε_c. Nevertheless we can make some statements. For the frequency range of our study the dispersive regime of ε_c extends down to temperatures about 20 K below $T_s(x)$. $\Delta\varepsilon$ is of the order of 3 just below $T_s(x)$. For $x=0.97$ and 0.84, τ follows approximately an Arrhenius law but with parameters considerably lower than above T_s, E_B is 540 and 390 K, f_A is 5 GHz and 10 MHz for $x=0.97$ and 0.84, respectively. For $x=0.79$, τ, however, increases on approaching T_s from below. This is incompatible with a thermally activated process, but is expected for the slowing down of critical fluctuations.

The secondary relaxations of ε_a occur at temperatures around 20 K. They are practically absent for $x=0.97$, still very weak for $x=0.84$ and $x=0.79$ with a dispersion step $\Delta\varepsilon$ of about 0.15 and finally grow to values of $\Delta\varepsilon$ of 0.6 for the samples with the lower methanol concentrations. Obviously the secondary relaxations are a property of partially occupied samples, only. The log f vs 1/T plots are not really linear, the average slope of these plots corresponds to barriers of the order of 100 to 200 K. α_{KWW} is around 0.5, suggesting broad distributions $g(\tau)$.

The primary relaxations of ε_a occur in the same T range as the relaxations of ε_c. In fact they have relaxation and Arrhenius parameters which are within the limited accuracy of the ε_a data identical to those obtained from ε_c. Thus they do not supply an independent piece of information and may simply originate from imprecise cutting of the sample plates, such that the dielectric signal is contaminated by ε_c. On the other hand, it is conspicuous that the dispersion step increases with decreasing x, in spite of the fact that ε_c decreases with decreasing x. Thus one cannot rule out the possibility that the primary relaxations of ε_a, similar to the secondary ones, are an intrinsic property of partially occupied samples.

DISCUSSION

The almost fully concentrated sample, $x=0.97$

First we concentrate on the $x=0.97$ sample, for which the largest amount of information exists and which also comes closest to the ideal case of a fully concentrated clathrate with the full translational and point symmetry of a crystal. In the high-T phase, the absence of birefringence within the ab plane and the x-ray diffraction results are consistent with the rhombohedral space groups $R\bar{3}$ and $R\bar{3}$ cited by previous authors. Most authors favor $R\bar{3}$ on the basis of dielectric, heat capacity, and NMR investigations, but the diffraction study and structure refinement of Mak[19] proposes $R3$ which means broken up-down symmetry and hence ferroelectricity. Our dielectric results and the absence of ferroelectric switching in our $P(E)$ curves strongly suggest a paraelectric state and hence $R\bar{3}$. The Curie constants M_c and $M_\perp$ obtained from fits to ε_c and ε_a supply the components μ_c and $\mu_\perp$ of the elementary dipole moment and hence its magnitude and angle ϑ with the c axis. $\mu_c=1.12$ D, $\mu=1.71$ D, $\vartheta=49°$. μ is close to the moment of the free methanol molecule (1.69 D), other contributions are obviously negligible. In particular one might have thought of a contribution from the protons of the OH hexagons which form the wall between a cavity and its next neighbor along c. The proton presumably has some freedom to move along the O-O bond, perhaps even in a double-well potential. However, we expect a kind of ice rule to hold which means that there should be only one, and not two or none, proton close to a given oxygen atom at any moment. Therefore the motion of the protons must be collective, all six protons moving clockwise or anticlockwise, such that any polarization within the basal plane is cancelled. The protons may move out of the plane of the hexagons,

thereby contributing to the response along c, but obviously this does not happen either, at least not for $x=0.97$. Also note that μ_c is larger than the projection of the moment of the free methanol molecule on the direction of its C-O bond ($=0.88$ D). Thus it is the full moment and not only its component along C-O which contributes to the paraelectric response and accordingly the origin of the primary relaxations are flips of the entire rigid molecule. The polar angle ϑ is in good agreement with the results of force field calculations[20] and with what has been deduced from NMR results,[9,10] which were however mainly sensitive to the orientation on the C-O bond. The estimate of ϑ had to be based on additional assumptions.

The fit of the modified Ising model to the data on ε_c supplies information on the coupling between the dipole moments. The coupling J_c along the chain is positive, that means of the ferroelectric-type, and two orders of magnitude larger than the coupling between the chains $J_\perp$. Thus the paraelectric response is almost perfectly that of a one-dimensional Ising system. The weak interchain coupling $J_\perp$ is antiferroelectric. The ferroelectric coherence length ξ along the chains can be estimated from the 1D Ising model $\xi^2/c^2=0.25\exp(4J_c/T)$, yielding a value of about $90c$ at 75 K where the experimental data start to deviate from the Ising behavior. The 1D character is not a consequence of largely different distances of next neighbors on the same chain and on different chains but is due to the EDD interaction in combination with the lattice symmetry. The EDD interactions along the chain add up and the coupling to neighboring chains decreases the longer the correlated regions along the chain in very much the same way as the magnetic field of the individual current loops does in a solenoid. Moreover the residual interaction between chains is highly frustrated because of the triangular arrangement of the chains. In fact the frustration would be complete if the molecules on neighboring chains were not displaced along c by $c/3$. For a completely ordered chain of dipoles aligned parallel to the chain and coupled by the EDD interaction, 83% of the total interaction strength come from first neighbors. J_c as obtained from the fit is 195 K, hence the contribution of one neighbor is about 160 K. The EDD interaction between two dipoles at a distance c with moments parallel to the c axis is 105 K for 1.12 D, the experimental value of μ_c, and 240 K for 1.69 D. Thus the magnitude of the coupling J_c is well accounted for by the EDD interaction. A detailed analysis would require a more realistic model which considers the canting of the moments and treats the lattice sums correctly.

On cooling, the static permittivity along c eventually deviates from the Ising behavior, passes through a maximum and slightly decreases toward T_s. This behavior is due to the onset of the 3D antiferroelectric interchain correlations. An individual chain would of course not order, but the weak, but nevertheless finite interchain coupling brings the transitions up to a temperature much higher than $J_\perp$, T_s being approximately determined by $T_s=|J_\perp|\exp(2J_c/T_s)$.

The permittivity results on the paraelectric phase show that ε_c and ε_a are well decoupled. Within the frequency range of the experiment, loss and dispersion appear in ε_c, only. Related effects in ε_a result from imperfect cutting. Thus our experiment does not supply information of possible flips of the perpendicular component $\mu_\perp$ about the c-axis by 120°. If such C_3 flips exist, they must remain fast compared to the measuring frequencies down to T_s. Complementary information on flips comes from the spin-lattice relaxation time of previous NMR experiments.[9,10] These data have been analyzed, as appropriate for a local probe, in terms of the local symmetry of the cage center which is C_{3i} for the $R\bar{3}$ lattice. C_3 flips are distinguished from inversion flips. The C_3 flips of the high-T phase were found to be thermally activated with an Arrhenius barrier of 350 K and an attempt frequency of 0.3 THz. The relaxation frequency at T_s calculated from these values is 1.4 GHz, which is indeed far beyond the frequency range of the present study. For the inversion flip of the methanol molecule the NMR studies give values of about 1200 K for the barrier and 20 THz for the attempt frequency ($110\ \mathrm{K}<T<200\ \mathrm{K}$), values which are much larger than what we determine from ε_c. Furthermore local inversion flips should not only show up in ε_c but also in ε_a. Note however that the permittivity probes the long-wavelength and not the local response. In the regime of dielectric dispersion ($T_s<T<78$ K) the ferroelectric correlations along c have grown to considerable length. Hence the flips relevant for ε_c are up-down flips of ferroelectrically correlated chain segments whereas the perpendicular component of μ is still disordered within such segments. For the relaxation rate f of the quasi-1D Ising model, one obtains $f=f_{\mathrm{loc}}[\cosh(2J_c/T)]^{-1}[\exp(-2J_c/T)-J_\perp/T]$.[21] Here f_{loc} is the relaxation rate which couples the individual dipole to the thermal bath. We assume $f_{\mathrm{loc}}=f_0\exp(-E_{\mathrm{loc}}/T)$ and think of the local barrier E_{loc} in terms of the crystal field of the cage. Using the values of J_c and $J_\perp$ derived from the static permittivity we fitted the expression for f to the effective Arrhenius law (with the parameters E_B and f_A) obtained from the HN analysis of dielectric dispersion and loss along c, treating E_{loc} and f_0 as free parameters. The values obtained are $E_{\mathrm{loc}}=320$ K, $f_0=0.16$ THz. This means that about 38% of the effective barrier, as determined from dielectric data, is due to the local crystal field, the remainder is due to the coupling J_c. As expected, the ferroelectric coupling slows down the relaxations at lower T both by lowering the effective attempt frequency and by increasing the effective Arrhenius barrier. Nevertheless this consideration cannot explain why the barriers obtained from NMR are so much higher than the effective barrier E_B of the present study.

The phase transition breaks the threefold symmetry about c. The condensation of the mode with the wave vector $\mathbf{q}_2$ at T_s suggests an antiferroelectric pattern of the low-T phase which consists of sheets of ferroelectric up and down chains, as predicted by Dansas and Sixou.[12] One up chain is surrounded by two up and four down chains. The additional modulation $\mathbf{q}_1$ is presumably due to a dimerization of the dipoles along the chain. In fact the r^{-3} dependence of the EDD interaction in combination with a shallow crystal field potential in the vicinity of the cage center with respect to shifts of the entire methanol molecule along c is likely to produce a dimerized state with alternating methanol-

methanol distances $c+d$ and $c-d$. The dimerization should develop already in the paraelectric phase in parallel with the ferroelectric correlations, where both types of 1D correlation should give rise to planes of diffuse intensity in reciprocal space. We have indeed observed weak traces of ferroelectric diffuse scattering in planes (hkl), l=integer but not at l=half-integer due to dimerization. The drop of ε_c at T_s is due to the formation of the long-range antiferroelectric arrangement of the ferroelectric chains. There are practically no ferroelectric fluctuations remaining below T_s. This is not surprising since already well above T_s the ferroelectric correlations have reached mesoscopic dimensions. The antiferroelectric ordering, however, continues below T_s as is evidenced by the growth of the intensities of the superlattice reflections and the residual T dependence of ε_a down to temperatures of the order of 20 K.

According to Matsuo[6] the entropy of transition per dipole (in units of k_B) is $\ln 2$. Hence the transition has been interpreted as an ordering of the up-down degree of freedom of Ising pseudospins. We disagree with both the value and the interpretation. We have not found a reliable way of splitting the total entropy $S(T)$ into contributions of the methanol molecules and of the host lattice by extrapolating the measured entropy of samples with different methanol concentration to $x=0$. Hence we have to limit the discussion to the apparent part ΔS in excess to a smooth background. From Fig. 9 one obtains an entropy of transition of $\ln 1.5$ per molecule and a change of entropy of $\ln 1.7$ from 50 K to temperatures just above T_s. In terms of the 6 orientations of μ in a C_{3i} site, the up-down degree of freedom is already eliminated by the one-dimensional short-range ferroelectric correlations in the paraelectric phase, leaving $\ln 3$ for the azimuthal motion. Obviously half of this is removed by the transition and the next 15 K below T_s. The remaining part (another $\ln 1.7$) is spread over the paraelectric phase and/or temperatures less than 50 K. Matsui *et al.*[10] conclude from their NMR results that the azimuthal reorientation of almost all methanol molecules disappears below T_s, on the other hand Ripmeester *et al.*[9] report residual C_3 reorientations in the low-T phase with an Arrhenius barrier as low as 115 K. This brings us to the secondary relaxations of the permittivity when the applied field is perpendicular to c. We could not extract reliable Arrhenius parameters from these relaxations for $x=0.97$ because of the weakness of the dispersion step and the loss, but the results on the other samples give barriers of the order of 100 to 200 K, quite in agreement with the NMR experiment of Ripmeester *et al.* For $x=0.97$, only a minute fraction of the dipoles contributes to these relaxations, presumably methanol molecules in irregular sites such as molecules next to vacant cavities or molecules in domain walls.

Finally some comments on the ferroelastic and martensitic aspect of the phase transition are in order. The rhombohedral-triclinic transition is of first order and can be classified as improper ferroelastic (ferroelastic species $\overline{3}F1$ [13]) with three domains. Upon cooling through the transition the samples do not shatter but rather stay intact. There are two types of boundaries to consider in which a lattice mismatch and hence strain energy can occur, the domain walls of the triclinic phase and the phase boundaries triclinic-rhombohedral in the T range of phase coexistence in the vicinity of T_s. For many types of ferroelastic transitions the accumulation of such strains over mesoscopic distances can be avoided by the formation of so-called zero net strain planes. The transformation strain can then be kept low by matching an appropriate multidomain pattern of the low-T phase to the lattice of the high-T phase in suitably oriented crystallographic planes. This mechanism does not work for the present transformation, simply because there are no zero net strain domain walls possible for the ferroelastic species $\overline{3}F1$.[22] Thus the system tries to keep the domain wall area at temperatures just below T_s small. Figure 12, upper frame, represents a cooling scan in which the sample enters the triclinic phase as monodomain and turns multidomain at T_s-5 K, as evidenced by the delayed splitting of the Bragg peak. The appearance of two, instead of three domains in Fig. 11 has the same reason. The transformation strains not only control the resulting domain pattern, but also affect the value of the spontaneous strain of the low-T phase, as can be seen from the jump of the peak position at T_s-5 K. This means that at this temperature the energy related to the strain mismatch is the same order as the difference of the volume free energies of the two phases.

Variation of the dielectric response with *x*, the partially occupied samples

The quasi-1D Ising model also supplies an excellent description of the high-T permittivity ε_c of the partially occupied samples. Therefore we continue to refer to this model for a while in spite of the fact that it applies to the nondiluted case, only. The coupling parameter J_c decreases with decreasing x, as expected of course from dilution, but the decrease is slower than $xJ_c(x=0.97)$. This points to a long, but not an infinite range of the interaction. The interchain coupling $J_\perp$ increases with decreasing x. This is highly unusual, but is due to a partial lifting of the frustration which in the fully occupied sample leads to an almost perfect cancellation of the interchain coupling. In spite of these changes the paraelectric high-T state of all samples can be still regarded as quasi-1D with the $J_c/J_\perp$ ratio decreasing from more than 10^2 for $x=0.97$ to about 15 for $x=0.40$. Even for $x=0.40$ the intrachain coupling is obviously still large enough to correlated the dipole moments over distances ξ along the chain of the order of some tens of lattice parameters c at the minimum temperature before the relaxations set in. This means that the ferroelectric coherence is not interrupted by individual empty cavities. Note that already for $x=0.84$ the average length of occupied chain segments between empty sites is reduced to about $5c$. The transition temperature T_s can be estimated from the values of J_c and $J_\perp$ via $T_s=|J_\perp|\exp(2J_c/T_s)$. For all samples, except $x=0.97$, one obtains values around 90 K. (For $x=0.97$ the estimated value of 71 K has little significance considering the enormous relative error of $J_\perp$.) Thus on the basis of this model, the effect of dilution on the coupling parameters, the decrease of J_c, and the increase of $J_\perp$ compensate each other.

The quasi-1D Ising model has also been setup for a low percentage of vacancies, but unfortunately for an intrachain coupling to next neighbors, only.[23] Here the coherence length is bound to the distance between empty cavities with the consequence that T_s drops rapidly with decreasing x. In fact, this model predicts that the transition should be already absent for $x=0.84$. Hence we consider the model for the concentrated case a better approximation to the experiment, but clearly a more realistic model considering the long range of the EDD interaction in combination with statistical site occupation is required.

For $x=0.97$ we have argued that the effective Arrhenius barrier is mainly due to the EDD coupling. This is not so for lower x. Following the procedure from above, the local Arrhenius parameters E_{loc} and f_0 can be extracted from the effective parameters E_B and f_A of the experiment. E_{loc} increases with decreasing x, while f_0 is about independent of x. For $x=0.40$, $E_{\mathrm{loc}}=625$ K, $f_0=0.11$ THz. Thus the effective barrier E_B of 815 K is mainly due to the local crystal field, leaving 190 K for the contribution from the coupling to neighboring dipoles. The value of 190 K is almost identical to J_c for $x=0.97$ ($=195$ K, see Table I) and reasonably close to $0.83J_c$ which is just the coupling strength to one next dipole. For $x=0.40$ the average length of occupied chain segments between vacancies is $2c$, meaning that a given dipole is likely to have just one next neighbor. This neighbor supplies a coupling of $0.83J_c$, higher ones supply contributions of the order of $0.1J_c$. Hence a value of 190 K is in fact what is expected for the contribution of the EDD interaction to the barrier at these low concentrations. This analysis suggest that even though the effective barrier E_B changes little with x, the partition into local and interaction related components does so drastically. The freezing of the dipoles at higher x is obviously controlled by the dipole interactions, whereas at lower x it has a more local character. The increase of E_{loc} towards lower x arises from the fact that the crystal field in a cavity is distorted by empty neighboring cavities perhaps via tilts of the benzene rings which form the side walls separating the cavities. In the terminology of disordered magnetic systems such effects which depend on the quenched occupation statistics are classified as random fields. In this sense the freezing changes from random bond dominated at higher x to random field dominated at lower x.

For $x=0.97$ the relaxations as probed by ε_c are almost monodispersive. For lower x the distributions of relaxation frequencies broaden significantly. For $x=0.40$ and 0.50, the full width at half maximum of the ε'' vs $\log(f)$ curve is about 3 decades (Fig. 15). Translating this width into a distribution of barrier heights gives a width of 270 K, while the mean value of E_B is 815 K. This variance of 270 K can be due to the crystal field part or to the interaction induced part of the barrier. The following estimate shows that both parts could be responsible. The change of the local barrier from 320 K for $x=0.97$ to 625 K for $x=0.40$, suggests that the variation of E_{loc} due to different configurations of occupied and empty neighbor cavities is of the order of 300 K. As far as the interactions are concerned, a dipole moment with no direct neighbors experiences a coupling of the order of $0.1J_c$, which is about 20 K, a dipole with two next neighbors but no higher neighbor a coupling of $1.66J_c$ or 320 K. This variation is again 300 K. Both types of broadening mechanism should scale roughly with $x(1-x)$. The fact that the width of the $g(\tau)$ distribution as represented by the HN and the KWW exponents varies with temperature points to an interaction dominated mechanism.

For $x=0.97$ we have argued that the residual primary and secondary relaxations appearing in ε_a are due to miscutting and to dipoles in irregular sites, respectively. For the samples with lower concentrations both types of relaxation increase in strength. At least for $x=0.50$ and $x=0.40$, where the maximum value of ε_c is about 50, only, one can definitely rule out that the primary relaxations appearing in ε_a are due to a misalignment of the electric field. It rather appears that they are an intrinsic effect. We ascribe them to dipoles which are not incorporated into ferroelectrically correlated chain segments. The inversion flips of such dipoles contribute to relaxations of ε_c as well as of ε_a. For the secondary relaxations, related arguments can be found: For $x=0.40$ and 0.50, but even for the samples with $x=0.84$ and 0.79, which still show long range ordering, there is a high degree of local disorder. Dipoles in the middle of correlated chain segments are locked in their azimuthal orientations by the coupling to the neighbors and can hence contribute to relaxations of ε_a only by collective rotational flips of the chain, a rather rare event for longer segments. Isolated dipoles, dipoles of short segments or at the end of long segments feel a much weaker coupling. At lower x, such dipoles are the rule rather than the exception.

CONCLUSIONS

For the almost concentrated sample the dielectric and structural behavior including dielectric relaxations and ordering is well described by the quasi-1D Ising model. The coupling parameters have been derived. In the paraelectric phase 1D ferroelectric correlations develop along chains running along the c axis. The 1D character is a consequence of the electric-dipole-dipole interaction in combination with a highly frustrated interchain interaction of the rhombohedral crystal structure. At some K above the phase transition temperatures, here the ferroelectric correlation length is already about $100c$, the antiferroelectric interchain correlations develop which then finally lead to a 3D long range ordered low-T phase. The low-T phase is a 2D triangular array of up and down chains. There are indications for a dimerization of the methanol molecules within the chains. The elementary dipole moment being practically identical to that of the free methanol molecule and the coupling being given by the bare EDD interaction, it should be possible to calculate the statics and the dynamics of the system almost from first principles (with the problem of the slow and conditional convergence of EDD lattice sums). In that respect, we consider this clathrate a model system for electrical ordering.

The clathrates tolerate fractional occupancies down to about $x=0.34$. The quasi-1D Ising model also accounts for the high-T dielectric response of the dilute samples, in spite of the fact that it ignores the effects of site occupation. Again 1D ferroelectric correlations along the chains reaching a

length of some tens of *c* units develop on cooling. For the three lower concentrated samples with $x < x_c \approx 0.76$, the antiferroelectric ordering no longer occurs and the dipoles freeze into the glassy state. We think of this state as a random array of ''block spins'' representing the total up or down dipole moment of the chain segments, the block spin being proportional to the length of the segment. The length of the segments can exceed the geometrical length of the chain between empty cages. This is a consequence of the long range of the EDD interaction. The coupling between block spins depends on their magnitude, orientation and relative position along *c* and is also subject to the inherent frustration of interacting dipoles on a lattice with threefold symmetry. The glassy freezing of the methanol clathrates shares the broad distribution of relaxation times with other examples of dipole glasses. In addition to what is known for other dipole glasses we could not only specify the microscopic interaction but could also estimate whether the freezing proceeds in local fields which vary from site to site due to different surroundings of empty and occupied neighbor sites (random field scenario) or is of the collective interaction dominated random bond type known from the spin glasses. The results favor the random field view for $x = 0.40$ and 0.50, whereas the sample with $x = 0.76$ is about half way between these cases. The dilute system would be ideally suited for computer simulations.

[1] K. Binder and A.P. Young, Rev. Mod. Phys. **58**, 801 (1986).
[2] U.T. Höchli, K. Knorr, and A. Loidl, Adv. Phys. **39**, 405 (1990).
[3] N.G. Parsonage and L.A.K. Staveley, *Disorder in Crystals*, (Clarendon, Oxford, 1978), Chap. 11.
[4] D.E. Palin and H.M. Powell, J. Chem. Soc. **1948**, 815 .
[5] T. Matsuo, H. Suga, and S. Seki, J. Phys. Soc. Jpn. **22**, 677 (1967).
[6] T. Matsuo, J. Phys. Soc. Jpn. **30**, 794 (1971).
[7] T. Matsuo and H. Suga, J. Inclusion Phenom. **2**, 49 (1984).
[8] H. Woll, M. Enderle, A. Klöpperpieper, M.C. Rheinstädter, K. Kiefer, F. Kruchten, and K. Knorr, Europhys. Lett. **51**, 407 (2000).
[9] J.A. Ripmeester, R.E. Hawkins, and D.W. Davidson, J. Chem. Phys. **71**, 1889 (1979).
[10] S. Matsui, T. Tserao, and A. Saika, J. Chem. Phys. **77**, 1788 (1982).
[11] E. Murakami, M. Komukae, T. Osaka, and Y. Makito, J. Phys. Soc. Jpn. **59**, 1147 (1990).
[12] P. Dansas and P. Sixou, Mol. Phys. **31**, 1297 (1976); **31**, 1319 (1976); Ber. Bunsen-Ges. Phys. Chem. **80**, 364 (1976).
[13] K. Aizu, J. Phys. Soc. Jpn. **27**, 387 (1969).
[14] D.J. Scalapino, Y. Imry, and P. Pincus, Phys. Rev. B **11**, 2042 (1975).
[15] R.V. Chamberlin, Phys. Rev. B **48**, 15 638 (1993).
[16] M. Dishon, G.H. Weiss, and J.T. Bendler, J. Res. Natl. Bur. Stand. **90**, 27 (1985).
[17] N. Menon and S.R Nagel, Phys. Rev. Lett. **74**, 1230 (1995).
[18] Z. Kutnjak, C. Filipic, A. Levstik, and R. Pirc, Phys. Rev. Lett. **70**, 4015 (1993).
[19] T.C.W. Mak, J. Chem. Soc. Perkin Trans. 2 **1982**, 1435 .
[20] V.E. Zubkus, I.L. Shamkovski, and E.E. Tornau, J. Chem. Phys. **97**, 8617 (1992).
[21] S. Zumer, Phys. Rev. B **21**, 1298 (1980).
[22] J. Sapriel, Phys. Rev. B **12**, 5128 (1975).
[23] D. Hone, P.A. Montano, T. Tonegawa, and Y. Imry, Phys. Rev. B **12**, 5141 (1975).